Research Article | Vol. 24, No. 26 | 26 Dec 2016 | OPTICS EXPRESS A1586

Optics EXPRESS

Symmetry-breaking nanostructures on crystalline silicon for enhanced light trapping in thin film solar cells

SEOK JUN HAN,[1,2] SWAPNADIP GHOSH,[2,3] OMAR K. ABUDAYYEH,[1,2] BRITTANY R. HOARD,[4] ETHAN C. CULLER,[4] JOSE E. BONILLA,[1] SANG M. HAN,[1,2,3,4] AND SANG EON HAN[1,2,4,*]

[1]*Chemical & Biological Engineering, University of New Mexico, Albuquerque, NM 87131, USA*
[2]*Center for High Technology Materials, University of New Mexico, Albuquerque, NM 87131, USA*
[3]*Electrical & Computer Engineering, University of New Mexico, Albuquerque, NM 87131, USA*
[4]*Nanoscience and Microsystems Engineering, University of New Mexico, Albuquerque, NM 87131, USA*
**sehan@unm.edu*

Abstract: We introduce a new approach to systematically break the symmetry in periodic nanostructures on a crystalline silicon surface. Our focus is inverted nanopyramid arrays with a prescribed symmetry. The arrangement and symmetry of nanopyramids are determined by etch mask design and its rotation with respect to the [110] orientation of the Si(001) substrate. This approach eliminates the need for using expensive off-cut silicon wafers. We also make use of low-cost, manufacturable, wet etching steps to fabricate the nanopyramids. Our experiment and computational modeling demonstrate that the symmetry breaking can increase the photovoltaic efficiency in thin-film silicon solar cells. For a 10-micron-thick active layer, the efficiency improves from 27.0 to 27.9% by enhanced light trapping over the broad sunlight spectrum. Our computation further reveals that this improvement would increase from 28.1 to 30.0% in the case of a 20-micron-thick active layer, when the unetched area between nanopyramids is minimized with over-etching. In addition to the immediate benefit to solar photovoltaics, our method of symmetry breaking provides a useful experimental platform to broadly study the effect of symmetry breaking on spectrally tuned light absorption and emission.

OCIS codes: (250.0250) Optoelectronics; (230.5298) Photonic crystals; (240.0310) Thin films.

References and links

1. B. C. Boots, EGY123A - Alternative Photovoltaic Solar Cell Technologies: Global Markets, BCC Research, 2014.
2. International Technology Roadmap for Photovoltaic (ITRPV), 6th Ed., http://www.itrpv.net/Reports/Downloads/.
3. M. S. Branham, W.-C. Hsu, S. Yerci, J. Loomis, S. V. Boriskina, B. R. Hoard, S. E. Han, and G. Chen, "15.7% Efficient 10-μm-thick crystalline silicon solar cells using periodic nanostructures," Adv. Mater. **27**(13), 2182–2188 (2015).
4. H. A. Atwater and A. Polman, "Plasmonics for improved photovoltaic devices," Nat. Mater. **9**(3), 205–213 (2010).
5. K. R. Catchpole and A. Polman, "Plasmonic solar cells," Opt. Express **16**(26), 21793–21800 (2008).
6. S. Pillai, K. R. Catchpole, T. Trupke, and M. A. Green, "Surface plasmon enhanced silicon solar cells," J. Appl. Phys. **101**(9), 093105 (2007).
7. H. R. Stuart and D. G. Hall, "Absorption enhancement in silicon-on-insulator waveguides using metal island films," Appl. Phys. Lett. **69**(16), 2327–2329 (1996).
8. E. Yablonovitch, "Statistical ray optics," J. Opt. Soc. Am. **72**(7), 899–907 (1982).
9. K. Vynck, M. Burresi, F. Riboli, and D. S. Wiersma, "Photon management in two-dimensional disordered media," Nat. Mater. **11**(12), 1017–1022 (2012).
10. A. Oskooi, P. A. Favuzzi, Y. Tanaka, H. Shigeta, Y. Kawakami, and S. Noda, "Partially disordered photonic-crystal thin films for enhanced and robust photovoltaics," Appl. Phys. Lett. **100**(18), 181110 (2012).
11. S. E. Han and G. Chen, "Optical absorption enhancement in silicon nanohole arrays for solar photovoltaics," Nano Lett. **10**(3), 1012–1015 (2010).

#277756 http://dx.doi.org/10.1364/OE.24.0A1586
Journal © 2016 Received 28 Sep 2016; revised 10 Nov 2016; accepted 12 Nov 2016; published 18 Nov 2016

Optics EXPRESS

12. L. Hu and G. Chen, "Analysis of optical absorption in silicon nanowire arrays for photovoltaic applications," Nano Lett. **7**(11), 3249–3252 (2007).
13. E. Garnett and P. Yang, "Light trapping in silicon nanowire solar cells," Nano Lett. **10**(3), 1082–1087 (2010).
14. M. D. Kelzenberg, S. W. Boettcher, J. A. Petykiewicz, D. B. Turner-Evans, M. C. Putnam, E. L. Warren, J. M. Spurgeon, R. M. Briggs, N. S. Lewis, and H. A. Atwater, "Enhanced absorption and carrier collection in Si wire arrays for photovoltaic applications," Nat. Mater. **9**(3), 239–244 (2010).
15. M. D. Kelzenberg, D. B. Turner-Evans, M. C. Putnam, S. W. Boettcher, R. M. Briggs, J. Y. Baek, N. S. Lewis, and H. A. Atwater, "High-performance Si microwire photovoltaics," Energy Environ. Sci. **4**(3), 866–871 (2011).
16. O. L. Muskens, J. G. Rivas, R. E. Algra, E. P. A. M. Bakkers, and A. Lagendijk, "Design of light scattering in nanowire materials for photovoltaic applications," Nano Lett. **8**(9), 2638–2642 (2008).
17. K. Peng, Y. Xu, Y. Wu, Y. Yan, S.-T. Lee, and J. Zhu, "Aligned single-crystalline Si nanowire arrays for photovoltaic applications," Small **1**(11), 1062–1067 (2005).
18. L. Tsakalakos, J. Balch, J. Fronheiser, B. A. Korevaar, O. Sulima, and J. Rand, "Silicon nanowire solar cells," Appl. Phys. Lett. **91**(23), 233117 (2007).
19. C. Lin and M. L. Povinelli, "Optical absorption enhancement in silicon nanowire arrays with a large lattice constant for photovoltaic applications," Opt. Express **17**(22), 19371–19381 (2009).
20. S. E. Han and G. Chen, "Toward the Lambertian limit of light trapping in thin nanostructured silicon solar cells," Nano Lett. **10**(11), 4692–4696 (2010).
21. A. Mavrokefalos, S. E. Han, S. Yerci, M. S. Branham, and G. Chen, "Efficient light trapping in inverted nanopyramid thin crystalline silicon membranes for solar cell applications," Nano Lett. **12**(6), 2792–2796 (2012).
22. P. Bermel, C. Luo, L. Zeng, L. C. Kimerling, and J. D. Joannopoulos, "Improving thin-film crystalline silicon solar cell efficiencies with photonic crystals," Opt. Express **15**(25), 16986–17000 (2007).
23. A. Chutinan, N. P. Kherani, and S. Zukotynski, "High-efficiency photonic crystal solar cell architecture," Opt. Express **17**(11), 8871–8878 (2009).
24. S. B. Mallick, M. Agrawal, and P. Peumans, "Optimal light trapping in ultra-thin photonic crystal crystalline silicon solar cells," Opt. Express **18**(6), 5691–5706 (2010).
25. J. N. Munday and H. A. Atwater, "Large integrated absorption enhancement in plasmonic solar cells by combining metallic gratings and antireflection coatings," Nano Lett. **11**(6), 2195–2201 (2011).
26. H. Sai, Y. Kanamori, K. Arafune, Y. Ohshita, and M. Yamaguchi, "Light trapping effect of submicron surface textures in crystalline Si solar cells," Prog. Photovolt. Res. Appl. **15**(5), 415–423 (2007).
27. P. Sheng, A. N. Bloch, and R. S. Stepleman, "Wavelength-selective absorption enhancement in thin-film solar cells," Appl. Phys. Lett. **43**(6), 579–581 (1983).
28. D. Zhou and R. Biswas, "Photonic crystal enhanced light-trapping in thin film solar cells," J. Appl. Phys. **103**(9), 093102 (2008).
29. M. Peters, C. Battaglia, K. Forberich, B. Bläsi, N. Sahraei, and A. G. Aberle, "Comparison between periodic and stochastic parabolic light trapping structures for thin-film microcrystalline Silicon solar cells," Opt. Express **20**(28), 29488–29499 (2012).
30. T. Cai and S. E. Han, "Effect of symmetry in periodic nanostructures on light trapping in thin film solar cells," J. Opt. Soc. Am. B **32**(11), 2264–2270 (2015).
31. J. Gjessing, A. S. Sudbø, and E. S. Marstein, "Comparison of periodic light-trapping structures in thin crystalline silicon solar cells," J. Appl. Phys. **110**(3), 033104 (2011).
32. C. Heine and R. H. Morf, "Submicrometer gratings for solar energy applications," Appl. Opt. **34**(14), 2476–2482 (1995).
33. Z. Yu, A. Raman, and S. Fan, "Nanophotonic light-trapping theory for solar cells," Appl. Phys., A Mater. Sci. Process. **105**(2), 329–339 (2011).
34. P. Campbell and M. A. Green, "Light trapping properties of pyramidally textured surfaces," J. Appl. Phys. **62**(1), 243–249 (1987).
35. P. Campbell, S. R. Wenham, and M. A. Green, "Light trapping and reflection control in solar cells using tilted crystallographic surface textures," Sol. Energy Mater. Sol. Cells **31**(2), 133–153 (1993).
36. C. Battaglia, C.-M. Hsu, K. Söderström, J. Escarré, F.-J. Haug, M. Charrière, M. Boccard, M. Despeisse, D. T. L. Alexander, M. Cantoni, Y. Cui, and C. Ballif, "Light trapping in solar cells: can periodic beat random?" ACS Nano **6**(3), 2790–2797 (2012).
37. M. S. Branham, W.-C. Hsu, S. Yerci, J. Loomis, S. V. Boriskina, B. R. Hoard, S. E. Han, A. Ebong, and G. Chen, "Empirical comparison of random and periodic surface light-trapping structures for ultrathin silicon photovoltaics," Adv. Opt. Mater. **4**(6), 858–863 (2016).
38. V. E. Ferry, M. A. Verschuuren, M. C. Lare, R. E. I. Schropp, H. A. Atwater, and A. Polman, "Optimized spatial correlations for broadband light trapping nanopatterns in high efficiency ultrathin film a-Si:H solar cells," Nano Lett. **11**(10), 4239–4245 (2011).
39. E. R. Martins, J. Li, Y. Liu, V. Depauw, Z. Chen, J. Zhou, and T. F. Krauss, "Deterministic quasi-random nanostructures for photon control," Nat. Commun. **4**, 2665 (2013).
40. C. Heine and R. H. Morf, "Submicrometer gratings for solar energy applications," Appl. Opt. **34**(14), 2476–2482 (1995).
41. S. V. Kesapragada and D. Gall, "Two-component nanopillar arrays grown by Glancing Angle Deposition," Thin Solid Films **494**(1–2), 234–239 (2006).

Optics EXPRESS

42. K. M. McPeak, C. D. van Engers, M. Blome, J. H. Park, S. Burger, M. A. Gosálvez, A. Faridi, Y. R. Ries, A. Sahu, and D. J. Norris, "Complex chiral colloids and surfaces via high-index off-cut silicon," Nano Lett. **14**(5), 2934–2940 (2014).
43. Y.-C. Chang, S.-C. Lu, H.-C. Chung, S.-M. Wang, T.-D. Tsai, and T.-F. Guo, "High-throughput nanofabrication of infra-red and chiral metamaterials using nanospherical-lens lithography," Sci. Rep. **3**, 3339 (2013).
44. C. Kittel, *Introduction to Solid State Physics*. 8th ed. (Wiley, 2004).
45. Y. Yin, Z.-Y. Li, and Y. Xia, "Template-directed growth of (100)-oriented colloidal crystals," Langmuir **19**(3), 622–631 (2003).
46. P. M. Bell, J. B. Pendry, L. M. Moreno, and A. J. Ward, "A program for calculating photonic band structures and transmission coefficients of complex structures," Comput. Phys. Commun. **85**(2), 306–322 (1995).
47. Z. Yu, A. Raman, and S. Fan, "Fundamental limit of nanophotonic light trapping in solar cells," Proc. Natl. Acad. Sci. U.S.A. **107**(41), 17491–17496 (2010).
48. D. F. Edwards, "Silicon (Si)"; D. W. Lynch and W. R. Hunter, "Silver (Ag)," in Handbook of Optical Constants of Solids, E. D. Palik, ed. (Academic, 1985).
49. S. Duttagupta, F. Ma, B. Hoex, T. Mueller, and A. G. Aberle, "Optimised antireflection coatings using silicon nitride on textured silicon surfaces based on measurements and multidimensional modelling," Energy Procedia **15**, 78–83 (2012).
50. W. Shockley and H. J. Queisser, "Detailed balance limit of efficiency of p-n junction solar cells," J. Appl. Phys. **32**(3), 510–519 (1961).
51. C. H. Henry, "Limiting efficiencies of ideal single and multiple energy gap terrestrial solar cells," J. Appl. Phys. **51**(8), 4494–4500 (1980).

1. Introduction

The large market share (~85%) of crystalline silicon (c-Si) solar cells is expected to continue in the near future [1], and the industry is rapidly moving towards thin crystalline film technologies. The benefit of using thin films is two-fold. The 1st benefit is reduced material cost. The c-Si wafers used in commercial solar cells today are typically 100-300 μm thick and constitute approximately 30–40% of total module cost [2]. The module cost in turn accounts for more than half of overall photovoltaic (PV) system cost [2]. Therefore, using thin (~10 μm) c-Si films would provide a substantial cost advantage. The 2nd benefit is reduced weight and contourability. Thin c-Si films can be supported on a light-weight flexible platform and contoured around the underlying structure. The weight reduction would decrease transportation and installation costs, thus providing savings in the overall balance-of-system costs [3]. While the cost benefits are clear, the optical absorption is significantly lower in thin c-Si films compared to thick films, hence highly efficient light trapping is necessary for thin films to achieve similar PV efficiency to thick films.

Various light-trapping schemes exist today to enhance light absorption. These schemes include light scattering by nanoparticles [4–7], random/quasi-random surface corrugation [8–10], nanorod arrays [11–19], and diffraction gratings [20–28]. When metal/dielectric nanoparticles are placed on thin films, light is efficiently scattered into the underlying films at the resonance frequencies. However, the metal nanoparticles strongly absorb light, when placed on weakly absorbing photoactive films [4]. This optical loss limits the light-trapping efficiency. Random surface roughening is another cost-effective manufacturing method to efficiently scatter light into the films. However, the inherent non-uniformity of random structures makes it difficult to optimize and improve both electrical and optical characteristics in PV applications [29]. Compared to the random surface features, the PV characteristics can be controlled more systematically by introducing periodic nanostructures, such as nanorod arrays or diffraction gratings. While nanorod-based solar cells can have strong light absorption, the surface recombination of charge carriers becomes a significant challenge due to the large surface-to-volume ratio [15]. In comparison, diffraction gratings have a smaller surface area than nanorods, while efficiently trapping light. Based on the evaluation of various light-trapping schemes and to judiciously exploit their advantages, we have selected metal-free, periodic, light-trapping nanostructures with a relatively small surface area increase (1.7 times) over a flat surface as a practical solution to achieve a high efficiency in thin-film solar cells.

Optics EXPRESS

Han *et al.* recently reported that proper breaking of point group symmetry in periodic nanostructures enhances light trapping [20, 30]. Throughout this work, we use the term "symmetry" to denote only the point group symmetry, excluding the translational symmetry. Breaking symmetry in periodic nanostructures can create new resonant absorption peaks and split degenerate absorption peaks, improving the light absorption integrated over the broad solar spectrum [30–33]. This improvement is very close to the Lambertian light-trapping limit and can reduce the c-Si solar cell thickness by two orders of magnitude, while achieving the same efficiency as thick flat c-Si films with an antireflection coating [20]. We note that symmetry breaking in macroscopic structures etched on off-cut Si wafers can also enhance light absorption, as Green *et al.* have demonstrated [34, 35]. However, the physics of enhancement in this case is fundamentally different. These macroscopic structures do not support resonance absorption, and light trapping can be explained by ray-tracing approximation. In contrast to Green's approach, our method eliminates the need for using expensive off-cut wafers in achieving symmetry-breaking surface corrugation.

Periodic and random structures have been compared for their light-trapping performance [29, 36, 37]. While the performance of the two is found to be similar to each other for silicon PV, the conclusion should be limited to the specific structures used in the studies. The reason is that depending on the geometry and scale, periodic structures may provide greater light trapping than random structures, and vice versa. Additional complexity in this comparison is that controlling the spatial correlation in random structures has been found to improve the light-trapping efficiency over both periodic and random structures [9, 10, 38, 39]. However, the correlation control requires rather expensive fabrication techniques. Here, we demonstrate that symmetry-breaking nanopyramid arrays provide a greater light-trapping efficiency than the symmetric nanopyramid arrays. The latter has been shown to be similar to random nanopyramids in light-trapping performance [37]. Therefore, we contend that symmetry-breaking periodic nanostructures offer a strong possibility to exceed the light-trapping efficiency of random nanostructures. In addition, our fabrication method is much less expensive than that of correlation control.

Symmetry-breaking nanostructures can be fabricated by directional dry etching [40], glancing angle deposition [41], wet etching on off-cut Si surfaces [35, 42], and multiple exposures in interference lithography [43]. However, fabricating such structures in a scalable, cost-effective, manufacturable manner remains elusive. In this work, we introduce a new approach to systematically break the symmetry in inverted nanopyramid arrays. The fabrication of symmetry-breaking nanostructures relies on simple, low-cost, wet-etch processing steps, and does not rely on the use of expensive off-cut Si wafers [35, 42]. This method also provides a convenient platform to rapidly canvass through a large range of geometries and study the effect of symmetry breaking on light trapping. In addition, the total increase in surface area is either comparable to the microscale inverted pyramids or much less than that of nanorod arrays. These advantages make the symmetry-breaking nanostructures exceptionally suitable for high-efficiency thin-film solar cells.

2. Results and discussion

Figure 1 illustrates our approach to break the symmetry in inverted nanopyramid arrays with each symmetry group denoted by the Schönflies notation. The left column of Fig. 1 shows a variety of etch templates represented by yellow mask with perforation. The open windows in the template are defined by lithography and dry etching. Interference or nanoimprint lithography can be used to define the submicron windows. The exposed underlying c-Si is then etched in an alkaline solution to create the inverted nanopyramids shown in the right column of Fig. 1. The fabrication technique is valid for single crystalline materials, but not for polycrystalline or amorphous materials. However, a metal layer deposited on the inverted nanopyramid arrays can be exfoliated and subsequently used as a bottom contact to deposit

Optics EXPRESS

polycrystalline or amorphous materials, making our approach widely applicable to non-crystalline films. This work will be discussed in our future publication.

In Fig. 1, we use a square lattice with C_{4v} symmetry as the basis of comparison, where one of the two lattice vectors is parallel to the [110] direction of the substrate [21]. The first level of symmetry breaking can be achieved by rotating the lattice vector of the etch template with respect to the [110] direction around the [001] axis (Fig. 1 inset). This lattice rotation effectively results in each inverted nanopyramid rotated around its own apex. Consequently, the mirror symmetry is completely broken while the 4-fold rotational symmetry is preserved. In addition to the rotation, the symmetry can be further broken by arranging the etch windows in non-square-lattice patterns. The possible two-dimensional non-square lattices are rectangular, triangular, centered-rectangular, and oblique lattices [44]. With the previously described sequence of symmetry breaking, we can reduce the symmetry of inverted nanopyramid arrays from C_{4v} to C_2.

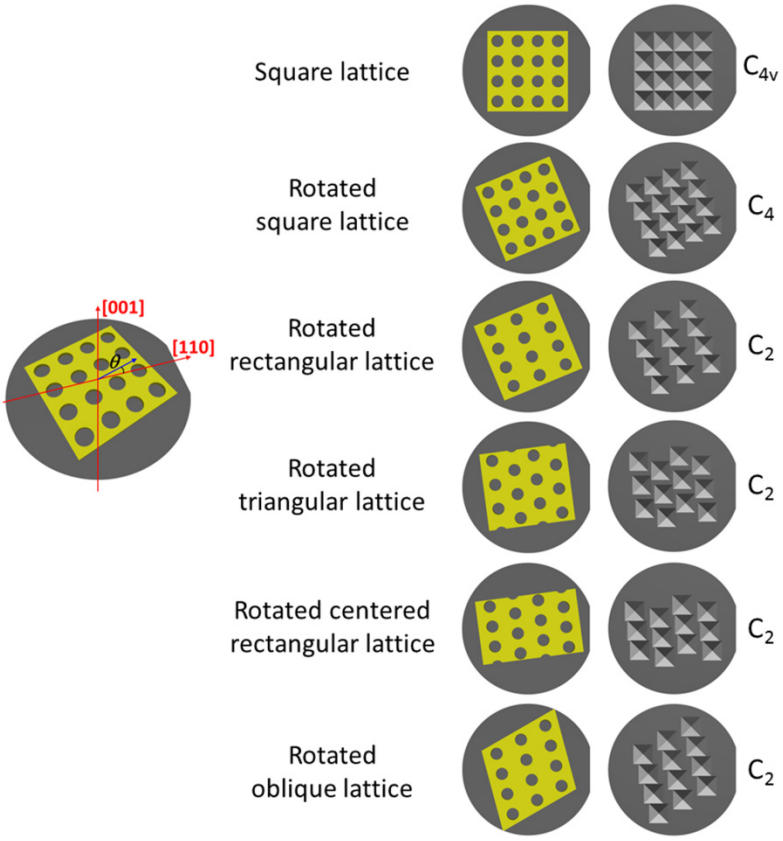

Fig. 1. Schematic approach to systematically break the symmetry by rotating the etch template (inset) and arranging the openings in various lattice types. Left figures show the etch template rotated about the [001] axis. The flat region on the right side of each c-Si wafer indicates the [110] direction. Subsequent etching in an alkaline solution defines inverted nanopyramids on c-Si(001) surfaces (right figures). The resulting symmetries are labeled in Schönflies notation.

The symmetry-breaking inverted nanopyramids can be directly fabricated on kerfless thin c-Si films. The c-Si films of a few μm to tens of μm in thickness are produced using a kerfless process and commercially available today. In this work, solely for the convenience of handling samples, we use silicon-on-insulator (SOI) wafers to obtain the light-trapping structures on thin c-Si films. The SOI wafers consist of a 10-μm-thick device layer, a 500-nm-thick buried SiO_2 layer, and a thick handle layer. The etch masks are fabricated on the device

Optics EXPRESS

layer of SOI wafers using interference lithography (IL) [Fig. 2(a) left]. The etch mask, going from top to bottom of its stack, is comprised of photoresist (NR7-500P, Futurrex), anti-reflection coating (ARC i-CON-16, Brewer science), and SiO_2. The 120-nm-thick SiO_2 layer is thermally grown on c-Si prior to lithography. Then, a 160-nm-thick anti-reflection layer and a 500-nm-thick photoresist film are sequentially spin-coated on SiO_2/Si. The photoresist was soft-baked at 150°C for 60 seconds, exposed to a laser with a wavelength of 355 nm (YAG-Nd laser, Infinity 40-100, Coherent Inc.) in Lloyd's mirror interferometry, and post-baked at 100°C for 60 seconds. After the photoresist is developed, reactive ion etching in CHF_3/O_2 plasma is used to create the etch windows in the SiO_2 layer. The SOI wafers with the etch masks are etched in an alkaline solution to define the inverted nanopyramids into the underlying c-Si, and the etch masks are subsequently removed [Fig. 2(a) middle]. The alkaline etch solution is prepared by dissolving 150 *g* of KOH in a mixture of 500 *ml* water and 125 *ml* isopropyl alcohol. Since the anisotropic etching step leaves flat unetched areas between the inverted pyramids, which reduce light trapping [21], we use a solution mixture of 70 wt% HNO_3 and 49 wt% HF (300:1 by volume) to further etch the c-Si isotropically [45]. Then, a 73-nm-thick silicon nitride (SiN_x) layer is deposited on the nanopyramids for antireflection, using plasma-enhanced chemical vapor deposition (PECVD). The refractive index of SiN_x layer is determined by ellipsometry to be 1.7 – 1.9 at the wavelength of 632.8 nm. A depression window is then created in the handle wafer using etching in a KOH solution over an area defined by lithography. To protect the front SiN_x layer and nanopyramids during the depression window etching, a polymer is spin-coated on the front surface prior to etching. The buried SiO_2 layer in the SOI wafer serves as the etch stop. After etching the depression window, the polymer protective film is removed, and a 100-nm-thick Ag film is deposited on the exposed surface of the SiO_2 layer as a backside reflector [Fig. 2(a) right]. In our current effort, we define the thin-film structures over a 2.5 cm × 1 cm area in SOI wafers. Similar procedures for preparing a thin c-Si film using SOI wafers can be found in References [3, 21].

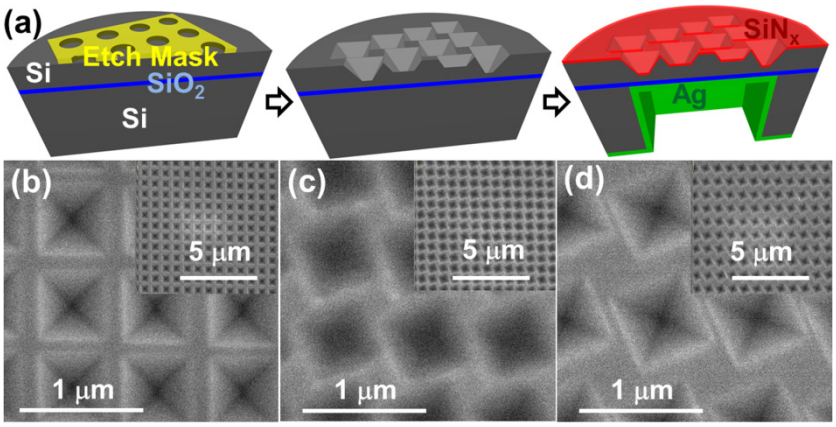

Fig. 2. (a) Illustration of fabrication process for light-trapping structures on thin c-Si films. (b)-(d) Scanning electron micrographs of the inverted nanopyramid arrays with (b) C_{4v}, (c) C_4, and (d) C_2 symmetry. The insets are a de-magnified view of each structure. These structures are obtained after 8-min anisotropic etching at 55°C followed by 10-min isotropic etching at 25°C. In (c) and (d), each pyramid is rotated by approximately 22.5° around its own apex from a lattice vector. The periodicity in the two orthogonal directions is 700 nm × 700 nm for (b)-(c) and 800 nm × 900 nm for (d).

Figures 2(b)-2(d) show inverted nanopyramid arrays with C_{4v}, C_4, and C_2 symmetry fabricated on SOI wafers before a SiN_x layer is deposited. The pitch in the square lattice is 700 nm for C_{4v} and C_4 symmetry. For C_2 symmetry, we make use of a rectangular lattice where the pitches along the lattice vectors are 800 and 900 nm, respectively. The C_4 and the C_2 structures are obtained by rotating the square and rectangular template lattices according to

Optics EXPRESS

our scheme in Fig. 1 (2nd and 3rd rows). The rotation angle is approximately 22.5°. This angle is chosen to be one half of 45° to reduce the symmetry from C_{4v} to C_4; 45° rotations would result in the same C_{4v} symmetry. The isotropic etching time is kept at 10 minutes to minimize the unetched area, while maintaining the shape definition of inverted nanopyramids. Prolonged isotropic etching tends to blur the shape of nanopyramids and makes it difficult to compare with modeling results. The resulting inverted nanopyramids show a long-range order. Figure 2 illustrates this uniformity over 10 μm range, and multiple scans over ~1 cm range at sampled regions show similar uniformity. Overall, we have established a systematic approach to break the symmetry in inverted nanopyramid arrays on c-Si(001) surface, using scalable lithography and simple wet etching steps.

The pitches of the three structures correspond to the maximum absorption for ~2-μm-thick c-Si films based on our optical calculations. To find the optimum pitches, we performed optical calculations based on transfer matrix method [46]. To save computation time in searching through many parameter values, we considered the nanostructures etched into a 2-μm-thick or 2.33-μm-thick c-Si film. For the C_4, and C_2 symmetry inverted nanopyramid arrays, the angle between one of the lattice vectors and the [110] direction is set to 22.5°. The inverted nanopyramid arrays are assumed to have no unetched horizontal areas by complete isotropic etching subsequent to KOH etching. The structures are conformally coated with a 60-nm-thick SiN_x layer with a refractive index of 1.9 for anti-reflection. On the backside of the c-Si film, a 717-nm-thick SiO_2 film and a 150-nm-thick Ag layer is placed as a reflector. Figure 3(a) shows the periodicity dependence of the calculated photovoltaic efficiency for the C_{4v} and C_4 symmetry inverted nanopyramid arrays on 2.33-μm-thick and 2-μm-thick c-Si films, respectively. Details of the photovoltaic efficiency calculation will be given later in this paper. In both cases, the optimized periodicity is found at 700 nm. Figure 3(b) displays the efficiency map of the C_2 symmetry (C_4 symmetry on the diagonal) structures for various combinations of periodicities from 500 to 1000 nm in the *x* and *y* directions, which correspond to the lattice vectors. This map reveals that the maximum efficiency occurs when the periodicities are 800 and 900 nm in the *x* and *y* directions, respectively. Thus, for maximum light trapping with inverted nanopyramids, the symmetry should be broken from C_4 to C_2 but not by a great degree of change in periodicity from that of C_4. The optimum periodicities found in the calculations are employed in our experiment in Figs. 2(b)-2(d). The calculated efficiencies at the optimum periodicities for C_{4v} (2.33 μm thickness), C_4 (2 μm thickness), and C_2 (2 μm thickness) symmetry inverted nanopyramids are 0.228, 0.237, and 0.251, respectively.

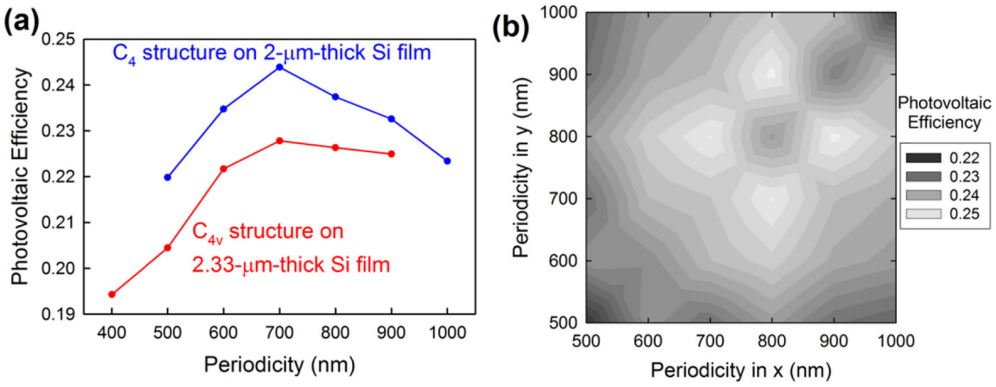

Fig. 3. (a) Calculated photovoltaic efficiency based on absorption in a 2.33-μm-thick and 2-μm-thick c-Si film for the C_{4v} and C_4 symmetry light-trapping structures, respectively, as a function of the periodicity. (b) Calculated efficiency for the C_2 symmetry structures based on a rotated rectangular lattice with various periodicities in *x* and *y* directions, where the angle between *x*-axis and [110] direction is 22.5°.

Optics EXPRESS

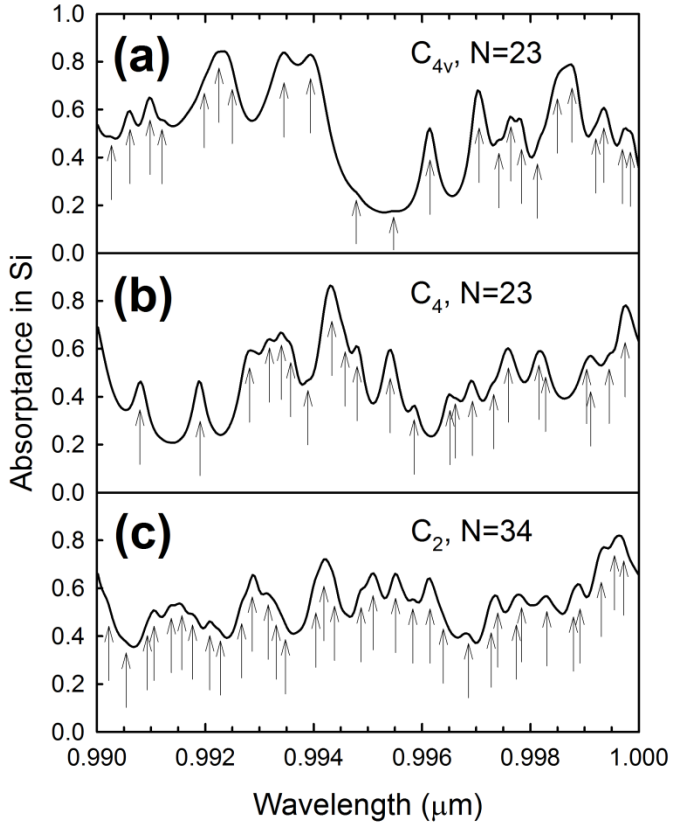

Fig. 4. Calculated spectra of absorption in a 10-μm-thick c-Si film for the C_{4v}, C_4, and C_2 symmetry light-trapping structures shown in Figs. 2(b)-2(d). Arrows indicate peak positions found from the second derivatives of the spectra.

Light absorption by the periodic structures is strongly governed by the number of resonance peaks and the coupling strength of the resonances to external radiation [30, 47]. In general, the number of peaks can be increased by breaking the symmetry, while the coupling strength is not trivial to control or estimate. Group theory predicts that, at normal incidence, the number of peaks, N, within a spectrum should be $N(C_{4v}) = N(C_4) < N(C_2)$ when N is large [30]. Using transfer matrix method [46], we calculate absorption spectrum from 0.99 to 1 μm for our 3 samples in Figs. 2(b)-2(d) and count N. Optical functions of the materials are taken from [48]. The large scale difference between the etch depth of ~0.5 μm and the film thickness of 10 μm poses a significant challenge in numerical calculations. To efficiently overcome the challenge, we use a layer-doubling technique in the transfer matrix method. In this technique, a transfer matrix for a thick Si layer is easily obtained by doubling the matrix for a thin layer multiple times. The calculated absorption spectrum is shown in Fig. 4. For accurate counting of the number of peaks, we use high spectral resolution at small intervals of 5×10^{-5} eV and take the second derivative of the spectrum. Peak positions are identified as the points where the second derivative is negative and locally minimum. In agreement with group theory, N increases from 23 for the C_{4v} and C_4 structures to 34 for the C_2 structure. For C_{4v} and C_4 symmetries, the optical response is the same for two orthogonal linear polarizations, resulting in degeneracy in the peaks. For C_2 symmetry, the 4-fold rotation symmetry is broken, and the degeneracy is lifted, resulting in resonance peak splitting and increased absorption. While the spectral range of investigation is very narrow, the results are a proof-of-concept demonstration of how the number of resonance peaks depends on the symmetry. Therefore, we expect the light absorption to increase as the symmetry is reduced

Optics EXPRESS

from C_{4v} (or C_4) to C_2. Moreover, as we will show later, the light absorption can increase despite the same number of resonance peaks (e.g., C_4 vs. C_{4v}) [30], if light coupling can be strengthened. As a result, the light absorption progressively increases as the symmetry is reduced from C_{4v} to C_4 to C_2.

We measure optical absorption of the C_{4v}, C_4, and C_2 symmetry samples, using a spectrophotometer with an integrating sphere (Lambda 950, Perkin-Elmer). The angle of incidence is 8° from the surface normal. Figures 5(a)-5(c) show the measured and calculated spectra of total absorption for the samples of C_{4v}, C_4, and C_2 symmetry, respectively. In general, good agreement between the measured and calculated absorption is observed. Calculated absorption in Ag is also displayed in Figs. 5(a)-5(c). The metal loss is appreciable only for wavelengths greater than 900 nm.

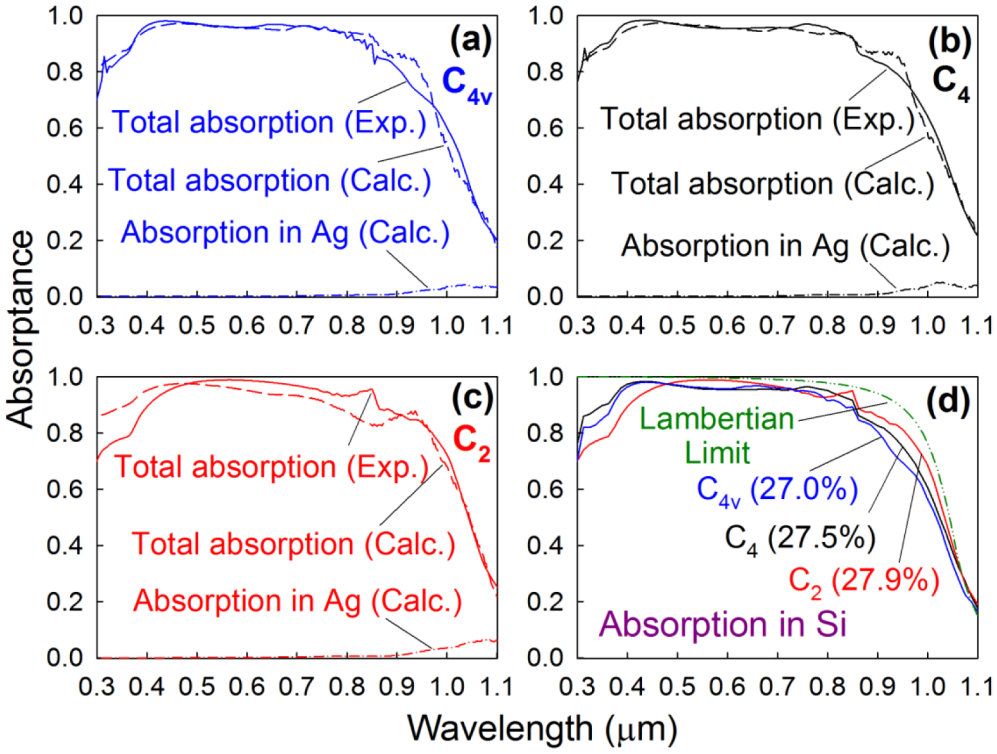

Fig. 5. (a)-(c) Comparison of experimental (solid line) and calculated (dashed line) total absorptance and calculated absorption in Ag (dot-dashed) for the inverted nanopyramid arrays of (a) C_{4v}, (b) C_4 and (c) C_2 symmetry shown in Figs. 2(b)-2(d). For the calculated absorption, the spectra are averaged over a photon energy range of 0.06 eV to smoothen sharp peaks. The refractive index of the SiN_x coating is 1.7 for (a), (b) and 1.9 for (c) in the calculations. (d) Absorptance in c-Si for the inverted nanopyramid arrays of C_{4v} (blue), C_4 (black), and C_2 (red) symmetry. The calculated photovoltaic efficiency for each nanopyramid structure is introduced in the parenthesis.

The absorption in c-Si is determined by subtracting the calculated absorption in Ag from experimentally measured total absorptance and is displayed in Fig. 5(d). Absorption in the SiN_x coating is negligible while it exhibits slight absorption below 0.4 μm in wavelength. When the refractive index of SiN_x films is relatively low (< 1.9) as found in our films, the solar weighted average absorption in the films is estimated to be less than 0.1% even over a corrugated surface [49]. Figure 5(d) shows that our systematic symmetry breaking along the $C_{4v} \rightarrow C_4 \rightarrow C_2$ sequence increases the absorption in c-Si in the long wavelengths, approaching closely to the Lambertian light-trapping limit [8]. For photovoltaic applications,

Optics EXPRESS

light trapping in the long wavelengths is important because the charge thermalization loss is minimal in these wavelengths. In short wavelengths, the C_2 symmetry sample exhibits absorption less than that of the others. We attribute the reason for this to the uncertainty in the refractive index of SiN_x films and the variation of the unetched areas [21]. To estimate the effect of symmetry breaking on the photovoltaic efficiency enhancement, we calculate the photovoltaic efficiency, using the spectra in Fig. 5(d). The efficiency calculation assumes that the charge carrier loss is due only to radiative recombination and that the solar cell is at room temperature. With this assumption, the current density J is given by

$$J(V) = \int_0^{\lambda_g} \frac{\lambda}{hc} A_{Si}(\lambda) I(\lambda) d\lambda + \frac{2\pi e E_g^{\,2} k_B T}{h^3 c^2} e^{-\frac{E_g}{k_B T}} \left(1 - e^{\frac{eV}{k_B T}}\right), \qquad (1)$$

where V, λ, h, c, A_{Si}, I, e, E_g, λ_g, k_B, and T denote voltage, wavelength, Planck's constant, light speed, absorption in c-Si, AM1.5G solar spectrum electronic charge, c-Si band gap, wavelength corresponding to the band gap, Boltzmann's constant, and solar cell temperature, respectively. The efficiency is the maximum JV product divided by incident power. When absorption is perfect, this efficiency leads to the Shockley-Queisser limit [50]. Note that Eq. (1) is different from Eq. (16) in [51]. This is because the substrate is a metal in our case, while [51] assumes an absorbing semiconductor substrate. The efficiencies for the C_{4v}, C_4, and C_2 symmetry samples are calculated to be 27.0%, 27.5%, and 27.9%, respectively. That is, the efficiency increases by the systematic symmetry breaking in the inverted nanopyramid arrays. The absolute increase of 0.9% in the efficiency by symmetry breaking could further increase when the corrugation structure is optimized and when the active layer thickness increases. For example, we consider the structures where the unetched flat areas between nanopyramids are completely removed by isotropic etching. In this case, the efficiencies for C_{4v}, C_4, and C_2 symmetry inverted nanopyramids on a 20-μm-thick silicon layer are estimated to be 28.1%, 29.1%, and 30.0%, respectively. This indicates that, if wet etching steps are further optimized, and the active layer thickness is doubled, our symmetry breaking method would increase the efficiency by 1.9%, a significant number for Si photovoltaics. Considering 15.7% device efficiency experimentally demonstrated by Han and his collaborators [3] from C_{4v} symmetry surface corrugation on 10-μm-thick substrates, we can extrapolate the device efficiency for our structures. For example, because the calculated efficiencies are 27.0% and 30.0% for a 10-μm-thick Si film with the C_{4v} symmetry structure and a 20-μm-thick Si film with the C_2 symmetry structure, one could potentially achieve 15.7% × 30.0 / 27.0 = 17.4% efficiency for 20-μm-thick solar cells with C_2 symmetry structures when flat areas between nanopyramids are minimal.

3. Conclusion

In conclusion, we have introduced a simple method to systematically break the symmetry on c-Si(001) surface for enhanced optical absorption in thin crystalline Si. This method makes use of cost-effective, manufacturable, wet etching steps directly applicable to kerfless thin Si films, and does not rely on the use of off-cut wafers. The symmetry of inverted nanopyramids can be reduced by rotating the etch template about the [001] axis and using five different etch window lattice types. Following this approach, the symmetry is reduced from C_{4v} to C_4 to C_2. Our experimental results show that the optical absorptance increases with the symmetry breaking. The accompanying calculations project that, as the symmetry of the inverted nanopyramids is broken in the $C_{4v} \rightarrow C_4 \rightarrow C_2$ sequence, the photovoltaic efficiency would increase along the path. We are currently working towards integrating our symmetry-breaking structures into c-Si solar cells according to the design provided by the US National Renewable Energy Laboratory. We expect that our method of symmetry breaking will be useful not only for light trapping, but also for spectrally tuned light absorption and emission. Our symmetry-breaking approach provides a versatile experimental platform to study the

Optics EXPRESS

effect of nanostructure symmetry on various optical material systems (e.g., organic photovoltaics and optoelectronic devices) and phenomena (e.g., high-Q resonance).

Funding

National Science Foundation (NSF) (1555290, 1635334, 1231046); Oak Ridge Associated Universities Ralph E. Powe Junior Faculty Enhancement Award.

Acknowledgment

We thank Dr. Pauls Stradins with the National Renewable Energy Laboratory for valuable discussions on c-Si photovoltaics.